Dynamic investigation of the finite dissolution of silicon particles in aluminum melt with a lower dissolution limit*

Dong Xi-Xi(董曦曦)[a)b)†], He Liang-Ju(何良菊)[a)c)], Mi Guang-Bao(弭光宝)[a)], and Li Pei-Jie(李培杰)[a)b)d)]

[a)] National Center of Novel Materials for International Research, Tsinghua University, Beijing 100084, China
[b)] Department of Mechanical Engineering, Tsinghua University, Beijing 100084, China
[c)] School of Aerospace, Tsinghua University, Beijing 100084, China
[d)] State Key Laboratory of Tribology, Tsinghua University, Beijing 100084, China

(Received 18 March 2014; revised manuscript received 5 June 2014; published online 24 September 2014)

The finite dissolution model of silicon particles in the aluminum melt is built and calculated by the finite difference method, and the lower dissolution limit of silicon particles in the aluminum melt is proposed and verified by experiments, which could be the origin of microinhomogeneity in aluminum–silicon melts. When the effects of curvature and interface reaction on dissolution are not considered; the dissolution rate first decreases and later increases with time. When the effects of curvature and interface reaction on dissolution are considered, the dissolution rate first decreases and later increases when the interface reaction coefficient (k) is larger than 10^{-1}, and the dissolution rate first decreases and later tends to be constant when k is smaller than 10^{-3}. The dissolution is controlled by both diffusion and interface reaction when k is larger than 10^{-3}, while the dissolution is controlled only by the interface reaction when k is smaller than 10^{-4}.

Keywords: silicon particle, aluminum melt, lower dissolution limit, finite dissolution model

PACS: 02.30.Jr, 02.70.Bf, 03.65.Vf, 61.25.Mv **DOI:** 10.1088/1674-1056/23/11/110204

1. Introduction

Dissolution is an important phase transformation process in fundamental science. For the dissolution of particles in metals, early models were proposed based on long-distance diffusion in the unbounded medium under the assumption of local equilibrium at the interface,[1,2] and the sharp interface model based on the separation of the constitutive phases and the phase field model derived from the minimization of the free energy functional were developed recently.[3,4] However, researchers mainly focused on the dissolution of particles in solid metals for the guide of heat treatment. For the dissolution in liquid metals, the solid could dissolve directly[5] if no inter-metallic compounds are formed, while the inter-metallic compounds first form in the interface and then dissolve[6] if inter-metallic compounds exist in the phase diagram, but some fundamental problems[7–10] about the dynamics and mechanism of dissolution in liquid metals are still unsolved.

The investigation of the structure of liquid metals was the cutting-edge topic of the interdiscipline between condensed matter physics and material science. X-ray diffraction, neutron scattering, and physical property measurement experiments were conducted to confirm the microinhomogeneity in certain liquid metal systems,[11–14] and molecular dynamics, *ab initio* molecular dynamics, and Monte Carlo simulations were used to reveal the property and structure of liquids or the evolution of liquid structure during solidification,[12,15–17] but seldom did researchers focus on the origin of microinhomogeneity in liquid metals from the view of dissolution.

The aluminum–silicon alloys have been implemented in a wide range of applications due to their high cast ability, high strength, and low coefficient of thermal expansion.[18] The investigation of the dissolution dynamics and mechanism of silicon particles in the aluminum melt was not only important for the smelting of aluminum–silicon alloys, but also important for the understanding of the long-time unsolved question about the origin and structure of microinhomogeneity in aluminum–silicon melts.[11,13,14,19] Previous studies[20–22] mainly focused on the dissolution of silicon particles in solid alloys for the instruction of heat treatment, while little work has been done on the dissolution of silicon particles in aluminum melt. The infinite[23] dissolution of primary silicon was studied,[24] but the dissolution tended to be finite[25,26] dissolution in reality, thus the finite dissolution model with a lower dissolution limit was developed in this article.

In this paper, the finite dissolution model of silicon particles with a large initial radius of 30 μm in the aluminum melt was built, the lower dissolution limit of silicon particles in the aluminum melt was proposed and verified by experiments, and the effects of curvature and interface reaction on finite dissolution were quantitatively investigated by the finite difference method.

*Project supported by the National Basic Research Program of China (Grant No. 2013CB632203).
†Corresponding author. E-mail: dongxx09@mails.tsinghua.edu.cn
© 2014 Chinese Physical Society and IOP Publishing Ltd

2. Lower dissolution limit of Si particle in Al melt

2.1. Model of lower dissolution limit

The size effect would appear when the silicon particles are dissolved from mesoscale to nanosacle in the aluminum melt, which results in a significant decrease in the melting point of silicon particles. Thus, we propose that the particle radius R_{T_m} with the melting point equal to the dissolution temperature is the lower limit of dissolution. When the radius of silicon particles is greater than R_{T_m}, the structure of silicon particles is relatively stable and dissolution happens. When the silicon particles are dissolved to be smaller than R_{T_m}, the structure of silicon particles is unstable and melting happens, and the melting of these nanoscale silicon particles that are wrapped by the transition layer could be the origin of nanoscale microinhomogeneity[13,14] in aluminum–silicon melts. Thus, the melting point of silicon particles in the aluminum melt is determined.

The melting point of silicon particles in the air[27] is

$$T_m^0 = T_0(1-\beta/2R), \tag{1}$$

where T_0 is the melting point of bulk silicon, β is a constant related to atomic spacing, and R is the radius of silicon particles.

Because of the surface tension, the silicon particles in the aluminum melt would suffer additional pressure $\mathrm{d}P$[28]

$$\mathrm{d}P = 2\sigma/R, \tag{2}$$

where σ is the surface tension between silicon particles and the aluminum melt.

According to the Clapeyron equation, the melting point of silicon particles in the aluminum melt would decrease by $\mathrm{d}T$[28]

$$\frac{\mathrm{d}P}{\mathrm{d}T} = \frac{\Delta_\alpha^\beta H_m}{T_m^0 \Delta_\alpha^\beta V_m}, \tag{3}$$

where $\Delta_\alpha^\beta H_m$ (46.4 kJ·mol^{-1})[29] and $\Delta_\alpha^\beta V_m$ (0.86456 cm^3·mol^{-1})[30] are the variation of molar enthalpy and volume accompanied with the melting of silicon.

Thus, the melting point of silicon particles in the aluminum melt yields

$$T_m = T_0\left(1-\frac{\beta}{2R}\right)\left(1+\frac{2\sigma}{R}\frac{\Delta_\alpha^\beta V_m}{\Delta_\alpha^\beta H_m}\right). \tag{4}$$

When substituting $T_0 = 1683$ K, $\beta = 1.88$ nm,[27] and $\sigma = 0.35241$ J/m^2[31] into Eq. (4), the lower dissolution limit of silicon particles in the aluminum melt is obtained, as shown in Fig. 1. When the dissolution temperature is 700 °C, the lower dissolution limit is 2.245 nm, and melting happens when the radius of silicon particles is dissolved to 2.245 nm.

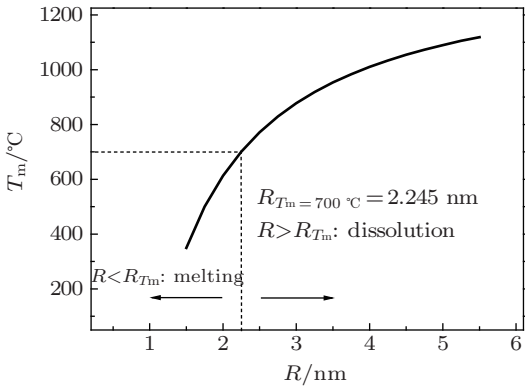


Fig. 1. Lower dissolution limit of Si particles in Al melt.

2.2. Experimental verification

In order to verify the above mentioned lower dissolution limit of Si particles in Al melt, the hypoeutectic Al–7 at.%Si, eutectic Al–12.2 at.%Si and hypereutectic Al–20 at.%Si binary alloys are chosen to give an integrated authentication, as shown in Fig. 2(a). The Al–12.2 at.%Si alloy is the eutectic composition that is composed of symbiotic Al and Si phases, and the hypoeutectic Al–7 at.%Si alloy consists of primary α-Al and eutectic Al and Si phases, while the hypereutectic Al–20 at.%Si alloy is composed of primary Si and eutectic Al and Si phases. It should be mentioned that the bond energy of Si–Si pairs (326.5 KJ·mol^{-1}) is significantly higher than that of the Al–Al pairs (186.2 KJ·mol^{-1}),[32] which means that the stability of the Si phase is higher than that of the Al phase, as revealed by the higher melting point of Si (1414 °C) than that of Al (660 °C). Therefore, for the melting of the hypoeutectic, eutectic, and hypereutectic Al–Si binary alloys, the Al phase first melts, while the Si phase first splits into small Si particles and then dissolves into the Al melt. Thus, the hypoeutectic Al–7 at.%Si, eutectic Al–12.2 at.%Si, and hypereutectic Al–20 at.%Si binary alloys are first melted by high-frequency induction melting to the temperature of about 800 °C in a Φ12-mm quartz tube under a vacuum of 3.3^{-3} Pa, then the three Al–Si melts are melt-spun to the copper roller with a diameter of 22 cm and a rotating speed of 32.8 ms^{-1}, and finally the final dissolution state of Si particles in Al melts was largely retained in the thin 40–50 μm thick melt-spun ribbons due to the rapid solidification process.

The SEM micrographs of the rapid solidified microstructure of hypoeutectic Al–7 at.%Si, eutectic Al–12.2 at.%Si, and hypereutectic Al–20 at.%Si binary alloys after induction melting to a temperature of about 800 °C are shown in Figs. 2(b)–2(d), respectively. Si particles with a diameter smaller than 10 nm can be found in all the hypoeutectic, eutectic, and hypereutectic Al–Si rapid solidified alloys, and the smallest Si particle is as small as 8 nm, as indicated by the arrows. According to the lower dissolution limit model in Section 2.1, the lower dissolution limit of Si particle radius in Al melt at

800 °C is 2.615 nm, i.e., the lower dissolution diameter is 5.23 nm. Considering that the cooling rate of the melt-spun process is in the range of 10^6–10^7 K/s, which cannot totally retain the final dissolution state of Si particles in Al melts, and Si particles will grow or even develop into a large Si phase during the rapid solidification process. Thus, the Si particles smaller than 10 nm that are found in the rapid solidified hypoeutectic Al–7 at.%Si, eutectic Al–12.2 at.%Si, and hypereutectic Al–20 at.%Si binary alloys are very close to the corresponding lower dissolution diameter given by the model, which verifies the correctness of the lower dissolution limit model proposed in Section 2.1.

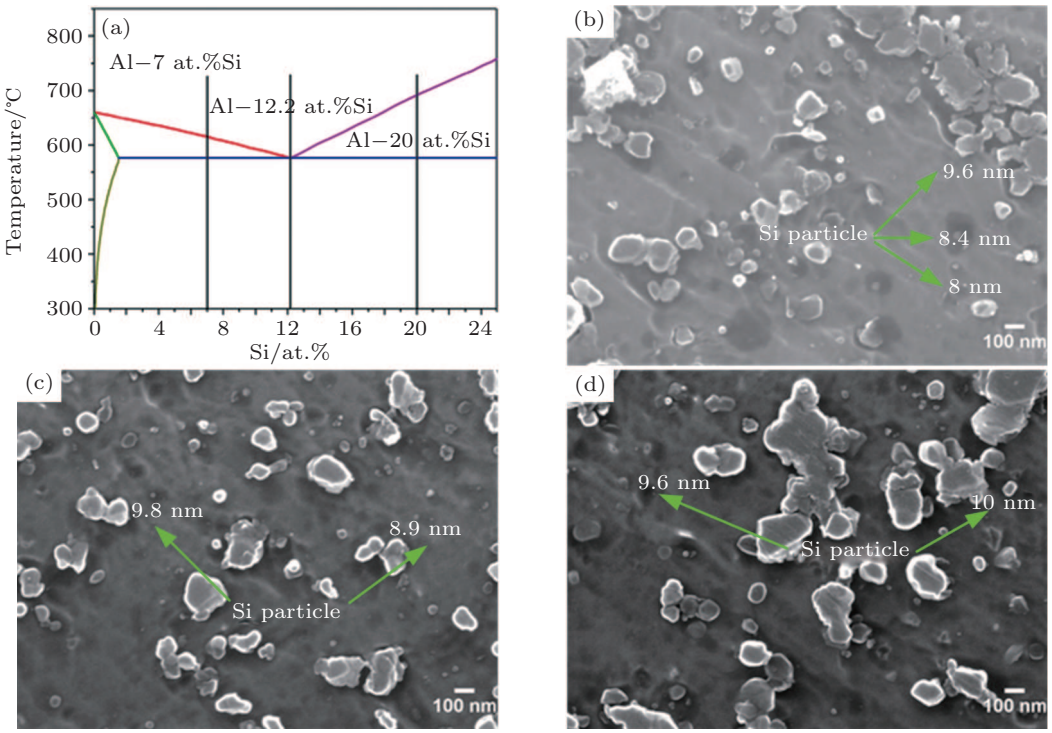


Fig. 2. (color online) Phase diagram of the Al–Si binary alloy (a) and SEM micrographs of the rapid solidified microstructure of Al–7 at.%Si (b), Al–12.2 at.%Si (c), and Al–20 at.%Si (d) binary alloys after induction melting.

3. Finite dissolution of Si particle in Al melt

3.1. Basic assumptions

(i) The silicon particles are spheres with the same size.

(ii) The liquid aluminum matrix is finite, and there is no mass transfer across the external boundary of the aluminum melt.

(iii) The diffusion coefficient is irrelevant with time and concentration.

(iv) The effect of convection is neglected.

3.2. Finite dissolution model

The dissolution tends to be finite dissolution in reality, so the dissolution model of silicon particles in finite aluminum melt is built, as shown in Fig. 3(a). Silicon particles with a

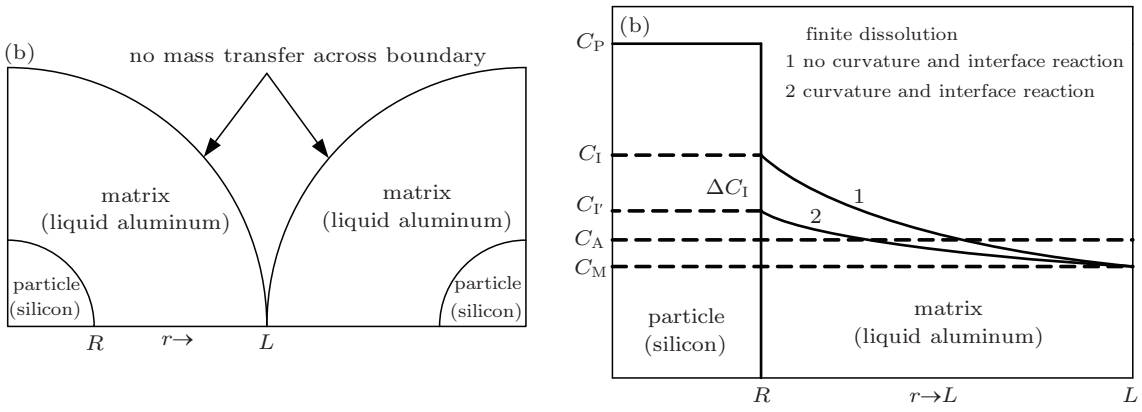


Fig. 3. Finite dissolution model of silicon particles in aluminum melt with (a) model description and (b) concentration distribution.

radius of R are dissolved in finite aluminum melt with the radius ranging from R to the external boundary L, and there is no mass exchange across the boundary. L is determined by the average concentration $C_{\rm A}$ of silicon (see Eq. (11)). Figure 3(b) shows the concentration distribution of silicon in finite aluminum melt, and Curves 1 and 2 represent the conditions that the effects of curvature and interface reaction on dissolution are not considered respectively. $C_{\rm P}$ and $C_{\rm M}$ are the concentration of silicon in the silicon particle and the liquid aluminum matrix respectively. $C_{\rm I}$ is the maximum solubility of silicon in aluminum in the liquid side of the interface at the dissolution temperature, and r is the radial distance between the liquid aluminum matrix and the center of the silicon particle.

3.3. No effects of curvature and interface reaction

3.3.1. Mathematical description

Diffusion in silicon particles and the liquid aluminum matrix conform to the second Fick's diffusion law[26]

$$\frac{\partial C^{\rm P}}{\partial t}=\frac{1}{r^2}\frac{\partial}{\partial r}\left(r^2D^{\rm P}\frac{\partial C^{\rm P}}{\partial r}\right), \tag{5}$$

$$\frac{\partial C^{\rm M}}{\partial t}=\frac{1}{r^2}\frac{\partial}{\partial r}\left(r^2D^{\rm M}\frac{\partial C^{\rm M}}{\partial r}\right), \tag{6}$$

where the superscript M and P represent the liquid aluminum matrix and silicon particles respectively, and they have the same meaning in subsequent equations.

The mass is conserved in the particle-matrix interface

$$(C_{\rm P}-C_{\rm I})\frac{{\rm d}R}{{\rm d}t}=D^{\rm M}\left(\frac{\partial C^{\rm M}}{\partial r}\right)_{r=R^+}-D^{\rm P}\left(\frac{\partial C^{\rm P}}{\partial r}\right)_{r=R^-}. \tag{7}$$

The boundary and interface conditions are

$$\left(\frac{\partial C^{\rm M}}{\partial r}\right)_{r=L}=0,\quad \left(\frac{\partial C^{\rm P}}{\partial r}\right)_{r=0}=0, \tag{8}$$

$$C^{\rm M}=C_{\rm I}\ \ (r=R^+),\quad C^{\rm P}=C_{\rm IP}\ \ (r=R^-), \tag{9}$$

where $C_{\rm IP}$ is the solubility of silicon in aluminum at the dissolution temperature.

The initial and geometrical conditions are

$$C^{\rm M}=C_{\rm M}\ \ (t=0,\ r>R_0),\quad C^{\rm P}=C_{\rm P}\ \ (t=0,\ r<R_0), \tag{10}$$

$$R_0^3C_{\rm p}+\left(L^3-R_0^3\right)C_{\rm M}=L^3C_{\rm A}. \tag{11}$$

3.3.2. Difference scheme description

There is no analytical solution for the finite dissolution, so the finite difference method is used to obtain the numerical solution. The silicon particle and the surrounding liquid aluminum matrix are dispersed into $N+1$ grid nodes numbered by $n=0,1,\ldots,m,\ldots,N$ along the radius direction, and node 0, m, and N represent the position of the center of silicon particles, the particle-matrix interface, and the external boundary of the liquid aluminum, respectively. The change rates of the concentration for a specific node in the silicon particle and the liquid aluminum matrix are

$$\frac{{\rm d}C_n^{\rm P}}{{\rm d}t}=\frac{\partial C_n^{\rm P}}{\partial r_n^{\rm P}}\left(\frac{{\rm d}r_n^{\rm P}}{{\rm d}t}\right)+\frac{\partial C_n^{\rm P}}{\partial t},\quad (n=1,2,\ldots,m-1), \tag{12}$$

$$\frac{{\rm d}C_n^{\rm M}}{{\rm d}t}=\frac{\partial C_n^{\rm M}}{\partial r_n^{\rm M}}\left(\frac{{\rm d}r_n^{\rm M}}{{\rm d}t}\right)+\frac{\partial C_n^{\rm M}}{\partial t},\quad (n=m+1,\ldots,N-1). \tag{13}$$

The relationship between the migration rate of the particle-matrix interface and a specific node in the silicon particle and the liquid aluminum matrix is

$$\frac{{\rm d}r_n^{\rm P}}{{\rm d}t}=\frac{r_n^{\rm P}}{R}\frac{{\rm d}R}{{\rm d}t},\quad (n=1,2,\ldots,m-1), \tag{14}$$

$$\frac{{\rm d}r_n^{\rm M}}{{\rm d}t}=\frac{L-r_n^{\rm M}}{L-R}\frac{{\rm d}R}{{\rm d}t},\quad (n=m+1,\ldots,N-1). \tag{15}$$

Substituting Eqs. (5) and (14) into Eq. (12), and Eqs. (6) and (15) into Eq. (13) yield

$$\begin{aligned}\frac{{\rm d}C_n^{\rm P}}{{\rm d}t}&=\frac{r_n^{\rm P}}{R}\frac{\partial C_n^{\rm P}}{\partial r_n^{\rm P}}\frac{{\rm d}R}{{\rm d}t}+D^{\rm P}\frac{2}{r_n^{\rm P}}\frac{\partial C_n^{\rm P}}{\partial r_n^{\rm P}}+D^{\rm P}\frac{\partial^2C_n^{\rm P}}{\partial r_n^{\rm P^2}},\\&\quad (n=1,2,\ldots,m-1),\end{aligned} \tag{16}$$

$$\begin{aligned}\frac{{\rm d}C_n^{\rm M}}{{\rm d}t}&=\frac{L-r_n^{\rm M}}{L-R}\frac{\partial C_n^{\rm M}}{\partial r_n^{\rm M}}\frac{{\rm d}R}{{\rm d}t}+D^{\rm M}\frac{2}{r_n^{\rm M}}\frac{\partial C_n^{\rm M}}{\partial r_n^{\rm M}}+D^{\rm M}\frac{\partial^2C_n^{\rm M}}{\partial r_n^{\rm M^2}},\\&\quad (n=m+1,\ldots,N-1).\end{aligned} \tag{17}$$

The difference scheme of Eqs. (16) and (17) is described as follows:

$$\begin{aligned}\frac{C_n^{j+1}-C_n^j}{\Delta t}&=\frac{n}{R^j}\frac{C_{n+1}^j-C_{n-1}^j}{2}\frac{R^{j+1}-R^j}{\Delta t}\\&\quad+D^{\rm P}\frac{m^2}{n}\frac{(C_{n+1}^j-C_{n-1}^j)}{(R^j)^2}\\&\quad+D^{\rm P}m^2\frac{\left(C_{n+1}^j-2C_n^j+C_{n-1}^j\right)}{(R^j)^2},\\&\quad(n=1,2,\ldots,m-1),\end{aligned} \tag{18}$$

$$\begin{aligned}\frac{C_n^{j+1}-C_n^j}{\Delta t}&=\frac{N-n}{L-R^j}\frac{C_{n+1}^j-C_n^j}{2}\frac{R^{j+1}-R^j}{\Delta t}\\&\quad+\frac{D^{\rm M}(N-m)}{[R^j+(n-m)(L-R^j)/(N-m)]}\frac{(C_{n+1}^j-C_{n-1}^j)}{L-R^j}\\&\quad+D^{\rm M}(N-m)^2\frac{\left(C_{n+1}^j-2C_n^j+C_{n-1}^j\right)}{(L-R^j)^2},\\&\quad(n=m+1,\ldots,N-1).\end{aligned} \tag{19}$$

The difference scheme of Eqs. (7) and (8) is

$$\begin{aligned}&(C_{\rm P}-C_{\rm I})\frac{R^{j+1}-R^j}{\Delta t}\\&=D^{\rm M}(N-m)\frac{4C_{m+1}^j-3C_{\rm I}-C_{m+2}^j}{2(L-R^j)}\\&\quad-D^{\rm P}\frac{m}{2}\frac{\left(C_{m-2}^j-4C_{m-1}^j+3C_{\rm P}\right)}{R^j},\end{aligned} \tag{20}$$

$$C_1^j=C_2^j,\ C_N^j=C_{N-1}^j. \tag{21}$$

3.4. Results and discussion

When the initial radius $R_0 = 30$ μm, the initial concentration $C_P = 1$ and $C_M = 0$, the geometrical condition $C_A = 0.16$, the interface condition C_I and C_{IP}, and the diffusion coefficient D (see Eq. (22)) are substituted into the difference equations and solved, the dynamic dissolution curve of silicon particles and the concentration distribution of silicon during dissolution were obtained, as shown in Fig. 3. From Fig. 4(a), the dissolution rate first decreases and later increases with time. From Fig. 4(b), the concentration gradient always exists in the aluminum melt, which indicates that the dissolution is controlled by diffusion

$$D = D_0 \exp(Q/R_g T), \tag{22}$$

where D_0 is 2.08×10^{-7} $m^2\cdot s^{-1}$,[33] Q is 25740 $J\cdot mol^{-1}$,[33] R_g is 8.314 $J\cdot mol^{-1}\cdot K^{-1}$, and T is the dissolution temperature ranging from 700 °C to 1100 °C.

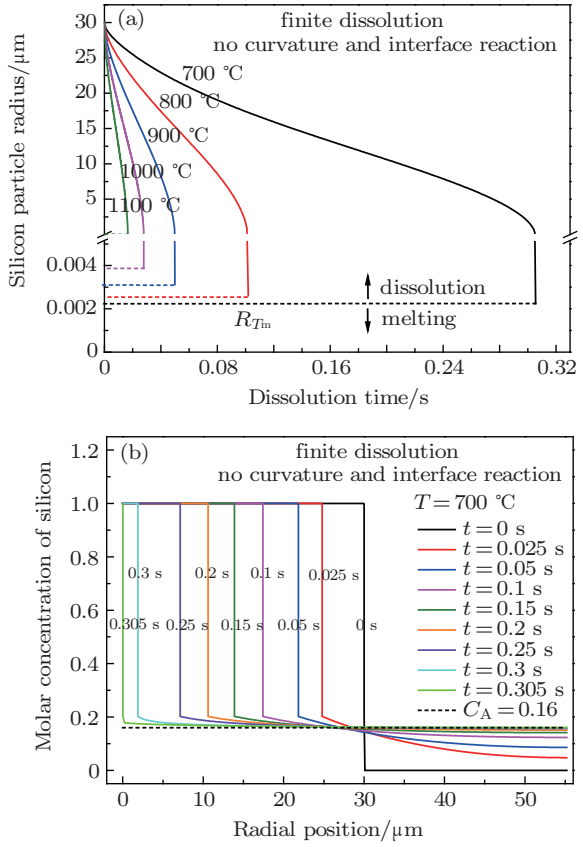


Fig. 4. (color online) Finite dissolution of silicon particles in aluminum melt without considering effects of curvature and interface reaction (a) dynamic dissolution curve and (b) concentration distribution.

3.5. Effects of curvature and interface reaction

The relationship between curvature and interface concentration is given by[34]

$$C_I(R) = C_I(\infty)\exp\left(\frac{2\gamma V}{RR_g T}\right), \tag{23}$$

where $C_I(\infty)$ is the interface concentration of the planar interface, γ is the interfacial free energy, and V is the molar volume of the particle. In this paper, γ and V are taken as 0.35241 $J\cdot m^{-2}$[31] and 12.04×10^{-6} $m^3\cdot mol^{-1}$,[29] respectively.

The interface reaction decreases the speed of the solute atoms from particles into the matrix, which results in the real interface concentration $C_{I'}$ that is lower than C_I by ΔC_I, as shown in Fig. 2. Aaron and Kotler[2] gave out the relationship between the dissolution rate dR/dt and ΔC_I when the separation of solute atoms from particles conform to the screw dislocation mechanism

$$\frac{dR}{dt} = -k(\Delta C_I)^2, \tag{24}$$

where k is the interface reaction coefficient. The smaller k is, the more difficult for the separation of solute atoms from particles into the matrix. Since the growth of the silicon phase in aluminum–silicon alloys conforms to the screw dislocation mechanism,[35,36] the inverse function of Eq. (24) could be used to reveal the effects of the interface reaction on the interface concentration

$$\Delta C_I = \sqrt{-\frac{1}{k}\frac{dR}{dt}}. \tag{25}$$

According to Eqs. (23) and (25), the interface concentration is obtained as

$$C_{I'}(R) = C_I(\infty)\exp\left(\frac{2\gamma V}{RR_g T}\right) - \sqrt{-\frac{1}{k}\frac{dR}{dt}}. \tag{26}$$

When substituting Eq. (26) into Eqs. (7) and (9) and considering a wide range of the interface reaction coefficient ($k = 10^{-5}$–10^{-1}), the dynamic dissolution curve of silicon particles is obtained (see Fig. 5). The dissolution rate first decreases and later increases with time when k is larger than 10^{-1}, and the curvature effect induced by the decrease in the particle radius at the later stage of dissolution could accelerate dissolution, as shown in Fig. 5(a). When k is smaller than 10^{-3}, the dissolution rate first decreases rapidly and later tends to be constant, which indicates that the effects of curvature could be neglected, as shown in Figs. 5(b)–5(d).

Figure 6 shows the concentration distribution of silicon in finite aluminum melt during dissolution when the effects of curvature and interface reaction are considered. From Figs. 6(a) and 6(b), when the interface reaction coefficient (k) is larger than 10^{-3}, the concentration gradient of silicon in the aluminum melt exists and decreases with time, which indicates that incomplete and non-uniform diffusion of the silicon happens in the aluminum melt, and the concentration gradient of silicon decreases with the decrease in k; thus the dissolution is controlled by both the diffusion and the interface reaction. From Figs. 6(c) and 6(d), when k is smaller than 10^{-4}, there is no concentration gradient of silicon in the aluminum melt, which reveals that the interface reaction rate is so slow that the silicon has enough time to conduct complete and uniform diffusion in the aluminum melt, thus the dissolution is controlled only by the interface reaction.

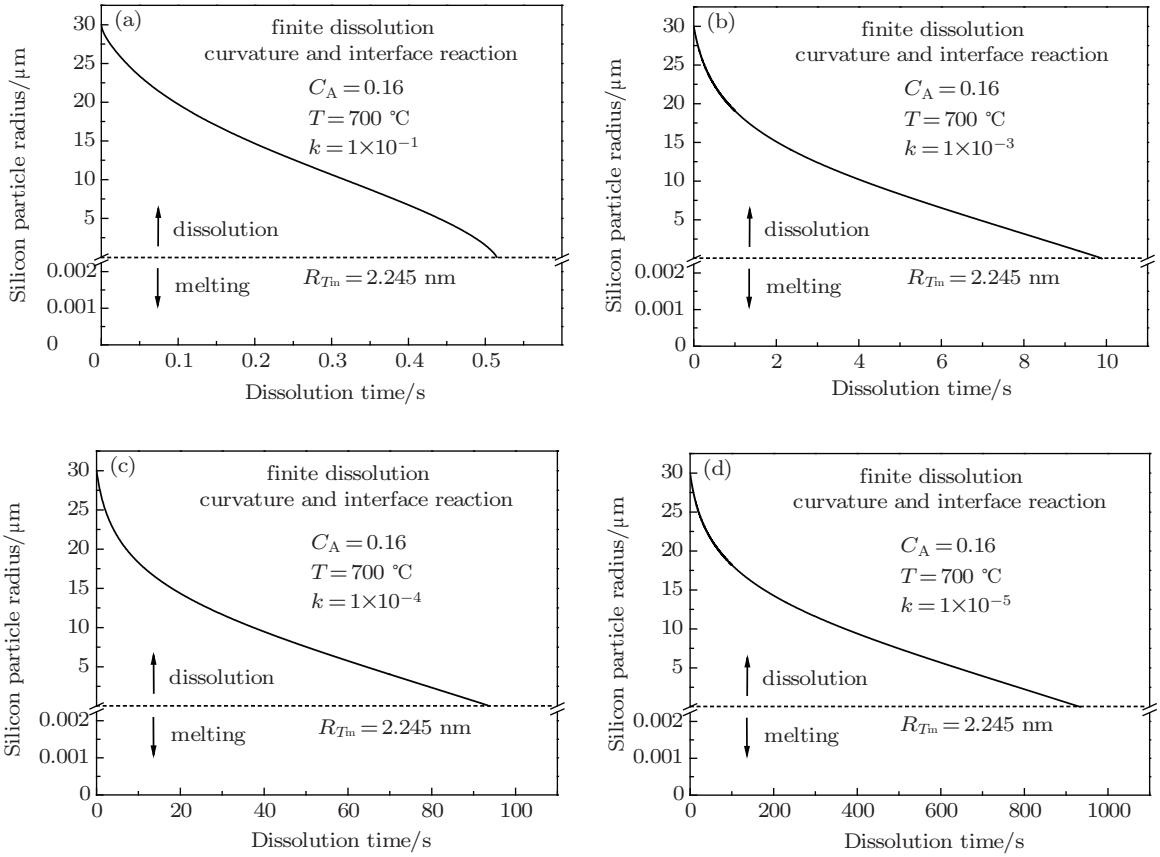


Fig. 5. Dynamic dissolution curve of silicon particles in finite aluminum melt considering the effects of curvature and interface reaction when the interface reaction coefficient k is equal to (a) 1×10^{-1}, (b) 1×10^{-3}, (c) 1×10^{-4}, and (d) 1×10^{-5}.

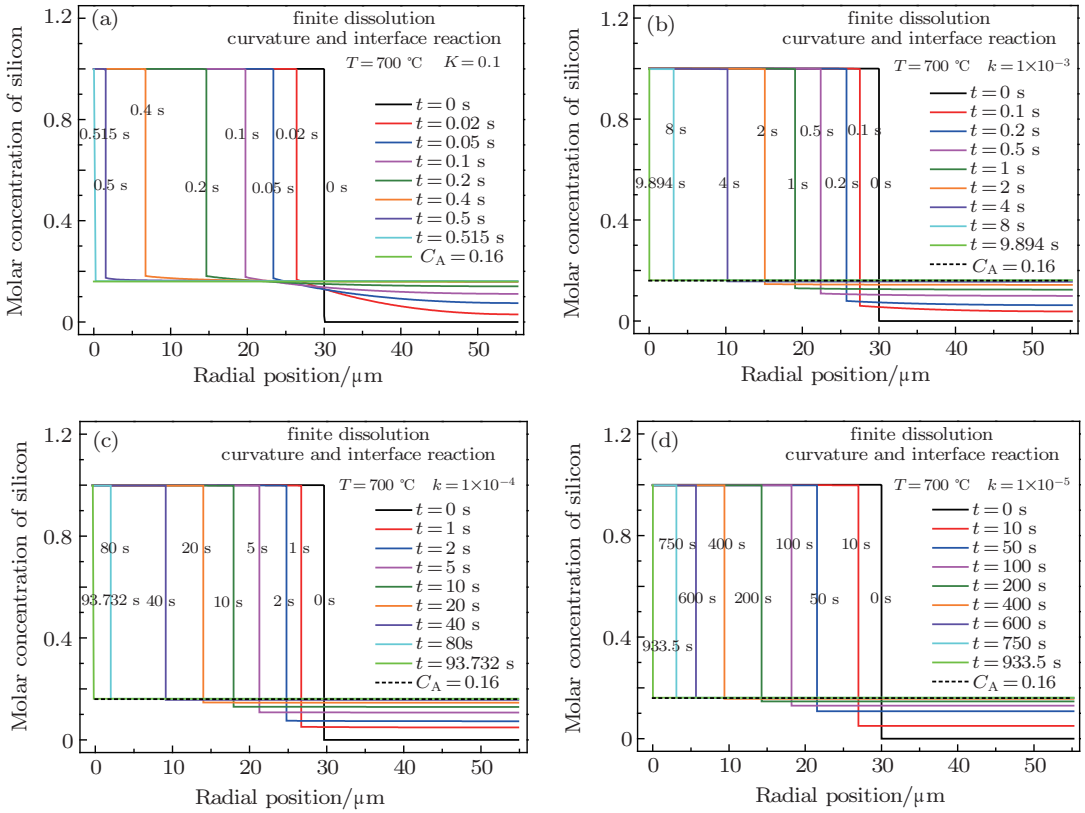


Fig. 6. (color online) Concentration distribution of silicon in finite aluminum melt during dissolution considering the effects of curvature and interface reaction when the interface reaction coefficient k is equal to (a) 1×10^{-1}, (b) 1×10^{-3}, (c) 1×10^{-4}, and (d) 1×10^{-5}.

4. Conclusions

(1) A model of the lower dissolution limit of silicon particles in the aluminum melt is proposed and determined, and the model is verified by experiments, which could be the origin of microinhomogeneity in aluminum–silicon melts.

(2) The finite dissolution model of silicon particles in the aluminum melt is built and calculated by the finite difference method, and the quantitative effects of curvature and interface reaction on the dissolution rate and dissolution mechanism are obtained.

(3) When the effects of curvature and interface reaction on finite dissolution are not considered, the dissolution rate first decreases and later increases with time.

(4) When the effects of curvature and interface reaction on finite dissolution are considered, the dissolution rate first decreases and later increases when the interface reaction coefficient (k) is larger than 10^{-1}, while the dissolution rate first decreases and later tends to be constant when k is smaller than 10^{-3}.

(5) The dissolution is controlled by both diffusion and interface reaction when k is larger than 10^{-3}, while the dissolution is controlled only by interface reaction when k is smaller than 10^{-4}.

References

[1] Whelan M J 1969 *Met. Sci. J.* **3** 95
[2] Aaron H B and Kotler G R 1971 *Metall. Trans.* **2** 393
[3] Vermolen F J, Javierre E, Vuik C, Zhao L and Zwaag S 2007 *Comput. Mater. Sci.* **39** 767
[4] Xu Z J and Meakin P 2008 *J. Chem. Phys.* **129** 014705
[5] Batchelor A W, Loh N L and Chandrasekaran M 2006 Materials Degradation and Its Control by Surface Engineering (2nd edn.) (London: Imperial College Press) pp. 161–164
[6] Pekguleryuz M O and Gruzleski J E 1989 *Metall. Trans. B* **20** 815
[7] Wu Q, Li S S, Ma Y and Gong S K 2012 *Chin. Phys. B* **21** 109102
[8] Ju Y Y, Zhang Q M, Gong Z Z and Ji G F 2013 *Chin. Phys. B* **22** 083101
[9] Zhang B H and Wu X P 2013 *Chin. Phys. B* **22** 056601
[10] Song C, Li D D, Xu Y C, Pan B C, Liu C S and Wang Z G 2014 *Chin. Phys. B* **23** 056801
[11] Srirangam P, Kramer M J and Shankar S 2011 *Acta Mater.* **59** 503
[12] Mauro N A, Bendert J C, Vogt A J, Gewin J M and Kelton K F 2011 *J. Chem. Phys.* **135** 044502
[13] Calvo-Dahlborg M, Popel P S, Kramer M J, Besser M, Morris J R and Dahlborg U 2013 *J. Alloy. Compd.* **550** 9
[14] Popel P S, Calvo-Dahlborg M and Dahlborg U 2007 *J. Non-Cryst. Solids* **353** 3243
[15] Wen D D, Peng P, Jiang Y Q, Tian Z A and Liu R S 2013 *Acta Phys. Sin.* **19** 196101 (in Chinese)
[16] Yang L, Bian X F, Pan S P and Qin J Y 2012 *Acta Phys. Sin.* **61** 036101 (in Chinese)
[17] Li Y D, Hao Q H, Cao Q L and Liu C S 2010 *Chin. Phys. B* **19** 086104
[18] Heard D W, Donaldson I W and Bishop D P 2009 *J. Mater. Process. Technol.* **209** 5902
[19] Khoo K H, Chan T L, Kim M and Chelikowsky J R 2011 *Phys. Rev. B* **84** 214203
[20] Tundal U H and Ryum N 1992 *Metall. Trans. A* **23** 445
[21] Vermolen F J, Slabbekoorn H M and Zwaag S 1997 *Mater. Sci. Eng. A* **231** 80
[22] Durbin T L 2005 *Modeling Dissolution in Aluminum Alloys* (Ph.D. Thesis) (Atlanta: Georgia Institute of Technology)
[23] Nojiri N and Enomoto M 1995 *Scr. Metall. Mater.* **32** 787
[24] Zhang R, Cao Q F, Pang S X, Wei Y and Liu L 2001 *Sci. Technol. Adv. Mater.* **2** 3
[25] Baty D L, Tanzilli R A and Heckel R W 1970 *Metall. Trans.* **1** 1651
[26] Tanzilli R A and Heckel R W 1968 *Trans. Metall. Soc. AIME* **242** 2313
[27] Wautelet M 1991 *J. Phys. D: Appl. Phys.* **24** 343
[28] Zhou L 2002 *Physical Chemistry Tutorials* (1st edn.) (Beijing: Science Press) pp. 164–254
[29] Li Z H 1985 *Element Properties Data Manual* (1st edn.) (Shijiazhuang: Hebei People's Publishing House) p. 14
[30] Inatomi Y, Onishi F, Nagashio K and Kuribayashi K 2007 *Int. J. Thermophys.* **28** 44
[31] Gunduz M and Hunt J D 1985 *Acta Metall.* **33** 1651
[32] Li P J 1995 *Structure and Heredity of Al–Si Alloys* (Ph.D. Thesis) (Harbin: Harbin Institute of Technology)
[33] Petrescu M 1970 *Z. Metallk.* **61** 14
[34] Min N B 1982 Physical Basis of Crystal Growth (1st edn.) (Shanghai: Shanghai Science and Technology Press) pp. 307–308
[35] Wang R Y, Lu W H and Hogon L M 1995 *Mater. Sci. Technol.* **11** 441
[36] Yilmaz F and Atasoy O A 1992 *J. Cryst. Growth* **118** 377